PERGAMON

International Journal of Heat and Mass Transfer 42 (1999) 4447–4460

International Journal of HEAT and MASS TRANSFER

www.elsevier.com/locate/ijhmt

Fourier analysis of conjugate gradient method applied to inverse heat conduction problems

M. Prud'homme, T. Hung Nguyen*

Department of Mechanical Engineering, École polytechnique de Montréal, CP 6079, Succ Centre-ville, Montréal, Quebec H3C 3A7, Canada

Received 13 July 1998; received in revised form 26 March 1999

Abstract

The convergence and regularization mechanism of the conjugate gradient algorithm applied to inverse heat conduction problems are studied within the context of a Fourier analysis, for a square enclosure subjected to an unknown time-varying heat flux on one side, and to known boundary conditions on the remaining sides. Analytic solutions are derived for the Fourier components of the unknown flux over a given time interval. The convergence rate of the algorithm is thereby shown to depend essentially on the time frequency of the data. Numerical solutions are also presented to describe in details the convergence process and solution regularization power of the conjugate gradient method, when the unknown heat flux contains many frequency components and the measurement data are noisy. It is found that an unknown time-dependent heat flux may be satisfactorily recovered using a single sensor even when the temperature field becomes two-dimensional, and that the sensor should be placed in a symmetric manner for better results.

1. Introduction

Inverse heat conduction problems are frequently encountered in many situations where the direct measurement of boundary conditions or the determination of thermophysical properties of solid bodies are impracticable. For example, while the heat flux at the outer surface of a re-entry vehicle cannot be measured directly, it may be estimated from temperature measurements underneath this surface by solving an inverse conduction problem (IHCP).

The first attempt to solve an inverse problem was made by Stefan who obtained an infinite series solution in 1890. Although the formulation and solution of this problem were presented over a century ago, it has grown rapidly as a research subject only during the last two decades or so. An excellent review of literature and comprehensive bibliography on the topic may be found in the books of Beck et al. [1] and Alifanov [2].

The main difficulty with inverse problems is due to their ill-posed character, in the sense of Hadamard [3]. That is, they may have no solution, or if a solution exits, it might not be unique or not continuous with respect to the given data. Therefore many techniques were proposed to regularize these problems. For example, Beck introduced the 'future time' method for IHCP, while Murio developed the 'mollification technique' to obtain smooth solutions of various inverse problems [4]. Tikhonov, Alifanov, and others from the Russian school proposed to cast the ill-posed inverse problem into an optimization problem with a regularized objective functional, and/or a self-regularizing algorithm of solution [2]. Along this avenue, it is well recognized that one of the most stable algorithms is the iterative conjugate gradient method (CGM).

* Corresponding author.

0017-9310/99/$ - see front matter
PII: S0017-9310(99)00112-X

Nomenclature

a_{ij}	polynomial coefficient
D	complex factor
E	object functional
H	height
k	thermal conductivity
P	polynomial
p	conjugate search direction
q	heat flux
Q_{ref}	reference flux value
S	active boundary
t	time
T	temperature
x, y	coordinates

Greek symbols

α	thermal diffusivity or step size
δ	Dirac delta function
Δ	increment
ε	small or random number
γ	coefficient
σ	random number
τ	variable
ω	frequency

Superscripts

k	iteration number
$\sim$	sensitivity variable
–	adjoint variable
*	complex conjugate

Subscripts

m	measurement value
0	reference value
f	final value

Other symbols

$\langle\cdot\vert\cdot\rangle$	inner product
$\Vert\cdot\Vert$	norm
$\vert\cdot\vert$	modulus
∇	gradient

Since the CGM has been used to solve a great variety of inverse problems [5,6,7,8], including IHCP, as well as problems of parameter determination and shape identification, it is worthwhile to examine, within the context of a Fourier analysis, how a solution is constructed via this algorithm.

To this purpose, the CGM will be applied first to a one-dimensional IHCP. Results will demonstrate the sequential recovery of the various frequency components of the unknown heat flux, which is at the heart of the regularizing mechanism embedded in the iteration process. In fact, both mathematical analysis and numerical computations will show how the low-frequency structure of an unknown heat flux is recovered after a few iterations, while high-frequency components are recovered only at a later stage. The effect of measurement errors will be analyzed next by introducing random noise in the input data. It will be shown that satisfactory predictions of the unknown heat flux may be obtained from noisy data, by stopping the iteration process before the undesirable high frequency components of the noise are recovered.

A two-dimensional IHCP will finally be solved to recover a uniform time-dependent heat flux. The effect of the sensor's positioning, as well as that of using several sensors, will be discussed. It will be shown that the sensor (or sensors) should be located with as much symmetry as possible within the cavity and that there is no need to use more than two sensors.

2. Problem definition

Let us consider the inverse conduction problem sketched in Fig. 1. Our purpose is to determine the unsteady flux $q(t)$ applied at $x=H$ over the time interval $0 \le t \le t_{\mathrm{f}}$, from temperature measurements T_{m}, taken at the sensor's position, for a given flux $q(y)$ applied at $x = 0$. It will be assumed throughout the discussion that the walls at $y = 0$, H are adiabatic and that the cavity is initially at temperature T_0 when heating begins. The IHCP may be expressed in a convenient non-dimensional form by introducing the definitions

$$T^* = \frac{T - T_0}{\Delta T}, \quad \Delta T = \frac{Q_{\mathrm{ref}} H}{k}, \quad (x, y)^* = \frac{(x, y)}{H}, \quad t^* = \frac{\alpha t}{H^2} \tag{1}$$

where all properties are evaluated at T_0. Omitting superscripts from now on, the temperature field within the cavity satisfies the unsteady dimensionless heat equation

$$\frac{\partial T}{\partial t} = \nabla^2 T \tag{2}$$

The IHCP can also be thought of as an optimization problem, of a type likely to be solved efficiently via the

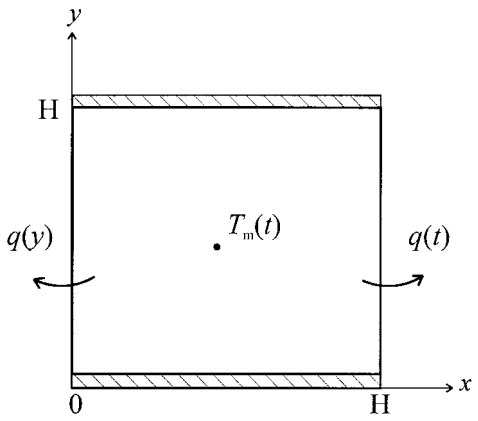

Fig. 1. Geometry and coordinate system.

conjugate gradient algorithm. It may then be stated in a formal way as:

given a set of temperature measurements $T_m(t)$ over the time interval $0 \le t \le t_f$, find the boundary heat flux $q(t)$ on surface S (the right wall) that will minimize the objective functional

$$E(q) = \frac{1}{2}\|T - T_m\|^2 \equiv \frac{1}{2}\int_0^{t_f} (T - T_m)^2 \, dt \tag{3}$$

It is understood that there may be one or many sensors, as needed, inside the cavity. If several sensors are used, the functional becomes the sum of individual contributions like Eq. (3) at each sensor location.

Minimization of Eq. (3) by CGM is achieved by constructing a sequence of approximations q^0, q^1, . . q^k, and so on, for the unknown heat flux according to $q^{k+1} = q^k + \alpha^k p^k$. Here α^k is the step size and p^k the conjugate search direction, which is related to the gradient of E with respect to the function q, and determined according to a well-known algorithm [9].

One step of the algorithm, in particular, is rightly devoted to the computation of the gradient. When some a priori representation is assumed for the flux, such as a linear combination of n known functions for instance, minimization of the objective functional is done over all possible coefficients of the combination. In this case, the parameter space over which minimization occurs is n-dimensional, and the gradient of E is nothing but the usual gradient in R^n. When no a priori information is available on $q(t)$, minimization must be achieved over an infinite-dimensional function space. In this case, the gradient of E and the step size α may be obtained respectively from the solution of the adjoint and sensitivity problems described below.

2.1. The sensitivity problem

Let us introduce the temperature sensitivity $\tilde{T}$ as the directional derivative of T at q in the direction Δq, i.e.

$$\tilde{T} = \lim_{\varepsilon \to 0} \frac{T(q + \varepsilon \Delta q) - T(q)}{\varepsilon} \tag{4}$$

Based on this definition, it is then straightforward to derive from Eq. (2) that the temperature sensitivity field is a solution of

$$\frac{\partial \tilde{T}}{\partial t} = \nabla^2 \tilde{T} \tag{5}$$

and must further satisfy the initial condition $\tilde{T} = 0$, the boundary condition

$$-\frac{\partial \tilde{T}}{\partial x}\bigg|_{x=1} = \Delta q(t) \tag{6}$$

and adiabatic conditions on the remaining walls, where the fluxes are known. It is finally noticed that the sensitivity problem, with Δq as the driving force, is linear just like the direct problem, and governed by the same equation.

2.2. The adjoint problem

When minimization occurs over an infinite-dimensional space, the gradient ∇E is related to the directional derivative of E by

$$D_{\Delta q} E(q) = \langle T - T_m \mid \tilde{T} \rangle = \langle \nabla E \mid \Delta q \rangle \tag{7}$$

where the inner products are defined from integrals [10], just as Eq. (3). It may be shown based on Eqs. (2), (3), (5), (6) and (7) that the gradient of the objective functional is equal to the so-called adjoint temperature $\bar{T}$ at the surface where the unknown flux is being sought, that is $\nabla E = \bar{T}(S, t)$. It is possible to derive for the adjoint temperature [2,3] the equation

$$\frac{\partial \bar{T}}{\partial t} = -\nabla^2 \bar{T} + \sum_i (T - T_m)\delta(\vec{r} - \vec{r}_i) \tag{8}$$

where the summation is carried out over all sensor positions $\vec{r}_i$. The adjoint temperature must here vanish at $t = t_f$, and satisfy adiabatic conditions on all the boundaries. The adjoint problem has non trivial solutions only as long as the error $T - T_m$, which appears as a set of point source terms in Eq. (8), is not zero. When the sensors are located on a boundary surface, say, on the left wall, the source terms may be dropped and Eq. (8) is then solved under the boundary condition

$$\left.\frac{\partial \bar{T}}{\partial x}\right|_{x=0} = T - T_{\mathrm{m}} \tag{9}$$

It is worth mentioning that, since the adjoint temperature vanishes at $t = t_{\mathrm{f}}$, the conjugate gradient method will always give $q^k(t_{\mathrm{f}}) = q^0(t_{\mathrm{f}})$, thereby convergence may be very slow if started with an unrealistic guess at t_{f}.

To solve the adjoint equation with the 'end condition' at the real physical time $t = t_{\mathrm{f}}$, one should first make the change of variable $\tau = t_{\mathrm{f}} - t$. Via this transformation, the adjoint problem becomes an initial value problem in τ with a positive diffusivity coefficient, which brings stability during computations [11].

3. Method of solution

The overall CGM algorithm may be summarized as follows.

1. Set initial conditions and choose initial guess q^0. Set iteration counter $k = 0$.
2. Solve the direct problem with q^k to obtain T^k.
3. Evaluate the error $T^k - T_{\mathrm{m}}$ at the sensors position(s).
4. Solve the adjoint problem backward in time to obtain $\bar{T}^k$.
5. Evaluate the gradient $\nabla E^k = \bar{T}^k(S, t)$.
6. Calculate the search direction p^k. If $k = 0$, $p^k = -\nabla E^k$, otherwise, $p^k = -\nabla E^k + \gamma^k p^{k-1}$ with

$$\gamma^k = \frac{\langle \nabla E^k - \nabla E^{k-1} \mid \nabla E^k \rangle}{\|\nabla E^{k-1}\|^2}$$

7. Solve the sensitivity problem with $\Delta q = p^k$ on surface S to obtain $\tilde{T}^k$ at the sensors position(s).
8. Calculate the step size

$$\alpha^k = -\frac{\langle \nabla E^k \mid p^k \rangle}{\|\tilde{T}^k\|^2}$$

9. Update to $q^{k+1} = q^k + \alpha^k p^k$.
10. Set $k = k + 1$, go back to step 2, repeat until convergence criterion $E^k < \varepsilon$ is satisfied.

A control volume approach based on a power-law scheme and a first-order implicit formulation was used to discretize the direct, sensitivity and adjoint equations. The resulting discrete systems were then solved by alternating line and column sweeps at each time step. The integrals involved in the definitions of the parameters α and γ were evaluated numerically using Simpson's method. Unless mentioned otherwise, all the computations were carried out starting from $q^0 = 0$ as initial guess for the flux, for a simulation time $t_{\mathrm{f}} = 1$, with a time step $\Delta t = \Delta\tau = 10^{-2}$, using a 21×21 uniform mesh.

4. Results and discussion

4.1. One-dimensional case

Since an arbitrary flux may be expanded in a Fourier series over a finite time interval $(0, t_{\mathrm{f}})$, the IHCP may be analysed without loss of generality for a single flux component of the form $q(t) = \mathrm{e}^{i\omega t}$. The regularization property of the conjugate method is then best understood, by careful consideration of the frequency response of the various solution elements during the first few iterations of the algorithm. This is easier done by assuming adiabatic conditions on the left wall, as the whole IHCP solution is then independent of the y coordinate.

Using Laplace transforms, the direct problem can be solved exactly under the above boundary condition. More details are provided in the Appendix, where it is also outlined how to deduce sensitivity and adjoint problem solutions from direct solutions, based on linearity principles and the existence of symmetry between the equations [10]. The temperature field is then

$$T(x, t) = -\frac{\mathrm{e}^{i\omega t}}{D}\cosh(\sqrt{i\omega}\,x) - \frac{i}{\omega} + 2\sum_{n=1}^{\infty}\frac{(-1)^n \mathrm{e}^{-n^2\pi^2 t}}{n^2\pi^2 + i\omega}\cos(n\pi x) \tag{10}$$

where D is a convenient short-hand notation for the complex quantity $\sqrt{i\omega}\sinh(\sqrt{i\omega})$. The solution therefore involves a phase shift in the harmonic term. Neglecting the rapidly decaying transient terms, the temperature measured by a sensor on the left wall at $x = 0$ is therefore

$$T_{\mathrm{m}}(t) = -\frac{\mathrm{e}^{i\omega t}}{D} - \frac{i}{\omega} \tag{11}$$

As D increases rapidly with frequency, the contribution of the harmonic term becomes negligible as soon as $\omega \approx 10$ or more. Let us now start the iteration process to recover $q(t)$ from the initial guess $q^0 = 0$, neglecting all transient terms from now on. The boundary condition for the computation of the first adjoint temperature field is then simply $T^0 - T_{\mathrm{m}} = -T_{\mathrm{m}}$. By using the symmetry and linearity properties mentioned earlier, the adjoint temperature at $x = 1$ in terms of τ is readily obtainable from Eq. (11). This yields

$$\bar{T}^0(1, t) = \frac{\mathrm{e}^{i\omega t_{\mathrm{f}}}}{D}\left(-\frac{\mathrm{e}^{-i\omega\tau}}{D^*} + \frac{i}{\omega}\right) + \frac{i}{\omega}P_1(\tau) \tag{12}$$

where P_1 is a linear polynomial whose coefficients are given in Appendix A. Using the explicit notation in terms of t

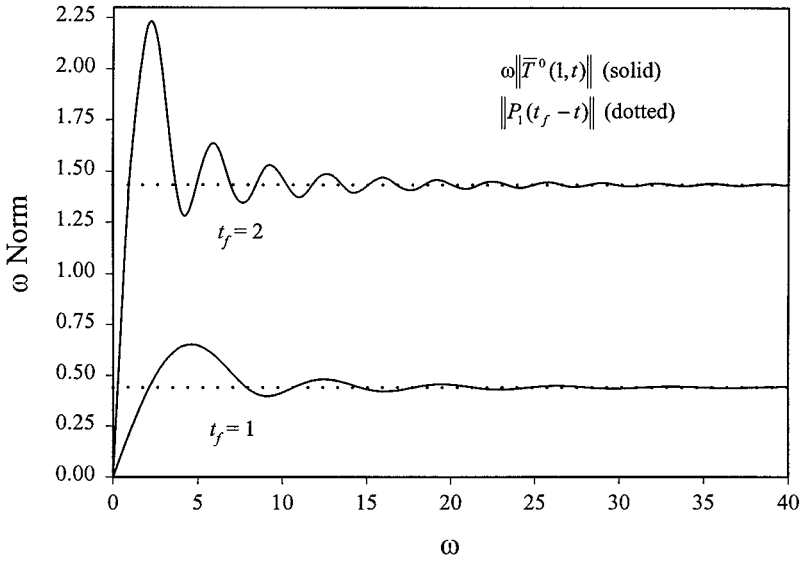

Fig. 2. Norm of adjoint temperature $\bar{T}^0$ vs frequency.

$$\bar{T}^0(1,t) = -\frac{e^{i\omega t}}{|D|^2} + \frac{ie^{i\omega t_f}}{\omega D} + \frac{i}{\omega}(t - t_f + 1/6) \tag{13}$$

it becomes clear that the harmonic term is in phase with, and proportional to, the unknown flux component.

Direct computation [10] shows that all terms on the right-hand side of Eq.(13) are of the same magnitude at low frequencies, when $\omega \approx 1$. For higher frequencies, the last term is much larger than the others. Consequently, the adjoint temperature becomes nearly inversely proportional to ω in such a way that the approximation

$$\omega\|\bar{T}^0(1,t)\| \approx \|P_1(t_f - t)\| \tag{14}$$

becomes valid as soon as $\omega \approx 10$ or more. This is confirmed in Fig. 2 as each plot levels out to the asymptotic value determined by t_f on the right-hand side. The presence of the damped oscillations in the profiles is the result of the occurrence of ωt_f in Eq. (13).

The temperature sensitivity at $x = 0$ is also found at once from the direct problem solution, giving

$$\begin{aligned}\tilde{T}^0(0,t) = {} & \frac{1}{|D|^2}T_m(t) \\ & - \frac{i}{\omega}\frac{e^{i\omega t_f}}{D}P_1(t) + \frac{i}{\omega}[a_{11}P_2(t) \\ & - P_1(t_f)P_1(t)]\end{aligned} \tag{15}$$

Once again, the last term on the right is the leading term at moderate frequencies. Taking out the real and imaginary parts of Eqs. (11), (13) and (15) gives the first iteration solutions for $q(t) = \cos(\omega t)$ and $\sin(\omega t)$, respectively. Considering the common asymptotic behavior of both $\tilde{T}^0$ and $\bar{T}^0$, the step size α^0 must be constant as ω increases. As a matter of fact, direct computations show that the value of α^0 remains nearly constant with frequency for a given t_f.

According to the solution algorithm, the new flux estimate is proportional to the adjoint temperature at $x = 1$. In compact form, one gets

$$q^1(t) = -\alpha^0\bar{T}^0(1,t) = A_1e^{i\omega t} + B_1t + C_1 \tag{16}$$

The coefficients in Eq. (16) are given by

$$\begin{aligned}A_1 &= \frac{\alpha^0}{|D|^2} \quad B_1 = ia_{11}\frac{\alpha^0}{\omega} \\ C_1 &= -i\frac{\alpha^0}{\omega}\left(P_1(t_f) + \frac{e^{i\omega t_f}}{D}\right)\end{aligned} \tag{17}$$

They are functions not only of ω, but also t_f, through the step size α^0. Since the latter is real, the coefficient A_1 does not generate any phase shift in the harmonic term, which becomes negligible (as well as part of C_1) as ω increases, so that the q^1 profile is then virtually a straight line.

The same steps may now be repeated to compute $q^2(t)$. Using linearity once more, Eq. (16) implies that $T^1(0,t) = A_1T_m(t) + B_1P_2(t) + C_1P_1(t)$ in the boundary condition $T^1 - T_m$ for the adjoint temperature $\bar{T}^1$. The latter is found by inspection from the boundary condition, after changing variables t to τ and expanding the polynomials P_1, P_2. This gives

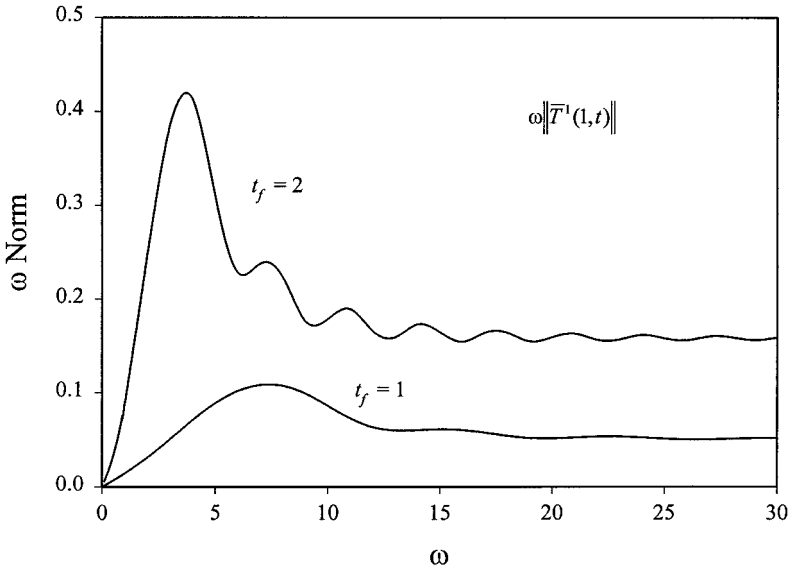

Fig. 3. Norm of adjoint temperature $\bar{T}^1$ vs frequency.

$$\bar{T}^1(1,t) = (1-A_1)\bar{T}^0(1,t) + F_1P_3(t_f - t) + F_2P_2(t_f - t) + F_3P_1(t_f - t) \quad (18)$$

where the coefficients

$$F_1 = B_1a_{22}$$

$$F_2 = -B_1(2a_{22}t_f + a_{21}) - C_1a_{11}$$

$$F_3 = B_1P_2(t_f) + C_1P_1(t_f) \quad (19)$$

are all linearly related to the A_1, B_1, C_1 of Eq. (17). This implies that, leaving aside the lowest frequencies, $\bar{T}^1$ will be inversely proportional to ω, just like $\bar{T}^0$. This is confirmed in Fig. 3, where the norm of the adjoint temperature is plotted for $t_f = 1$ and 2.

For the second iteration, the conjugate direction is given by $p^1 = -\bar{T}^1 - \gamma^1\bar{T}^0$. Rearranging terms in Eq. (18) therefore yields

$$p^1 = (A_1 - 1 - \gamma^1)\bar{T}^0(1,t) + G_1t^3 + G_2t^2 + G_3t + G_4 \quad (20)$$

It can be verified that γ^1 is a small quantity and that the new conjugate direction remains very close to the adjoint temperature $\bar{T}^1$. The coefficients G_i in Eq. (20) are defined in terms of the previous F_i as

$$G_1 = a_{33}F_1$$

$$G_2 = -(3a_{33}t_f + a_{32})F_1 - a_{22}F_2$$

$$G_3 = (3a_{33}t_f^2 + 2a_{32}t_f + a_{31})F_1 + (2a_{22}t_f + a_{21})F_2 + a_{11}F_3$$

$$G_4 = -F_1P_3(t_f) - F_2P_2(t_f) - F_3P_1(t_f) \quad (21)$$

From Eq. (20), the temperature sensitivity is found by inspection, once more, as

$$\tilde{T}^1(0,t) = (1+\gamma^1 - A_1)\tilde{T}^0(0,t) + G_1P_4(t) + G_2P_3(t) + G_3P_2(t) + G_4P_1(t) \quad (22)$$

The step size α^1 is now a complex quantity. It can be seen from Fig. 4 that the step size is determined only by t_f at high frequencies, although it is far from being constant at low frequencies. The new flux estimate $q^2 = q^1 + \alpha^1p^1$ can be expressed from Eqs. (16) and (20) as

$$q^2(t) = \left[1 + \frac{\alpha^1}{\alpha^0}(1+\gamma^1 - A_1)\right]q^1(t) + \alpha^1(G_1t^3 + G_2t^2 + G_3t + G_4) \quad (23)$$

Figs. 5–7 show for $q(t) = -\sin(\omega t)$ a comparison of the analytic solutions above with their numerical counterparts, including the transients. The computations were all carried out for a sensor placed on the left boundary, using 41×21 meshes.

The agreement is satisfactory overall for the first update q^1, as displayed in Fig. 5, with a slight discrepancy near $t = 0$, where the transients of T_m are present, and also near $t = t_f$, where the transients of $\bar{T}^0$ are also present. It can be noticed that q^1 is far

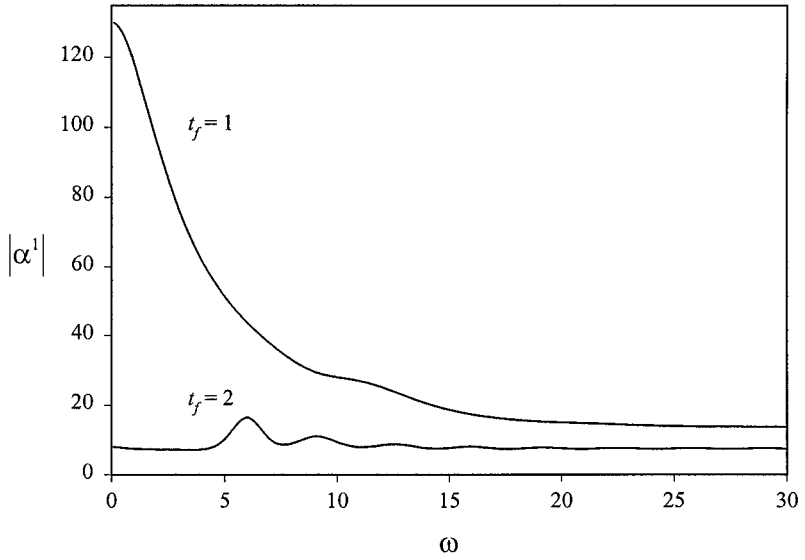

Fig. 4. Step size modulus vs frequency.

from being zero at $t = 0$, as the exact flux does. Nevertheless, the second iteration predicts a much more realistic flux profile, with a fair sinusoidal shape. As far as the numerical solution is concerned, the unknown flux is thus reasonably well recovered after only two iterations. But the analytic solution is not as satisfactory for the second update as it was for the first one. The greater discrepancy might well be caused by the cumulative effect of the transients of T_m, $\bar{T}^0$ and $\tilde{T}^0$, as suggested by Fig. 6, where the agreement is much better over the longer simulation time $t_f = 2$.

Fig. 7 shows the same quantities as Fig. 6, but for $\omega = 10\pi$. The plot for the first update solution is practically a straight line on the graph, showing that the linear term in Eq. (13) is now dominant. The amplitude is also one order of magnitude smaller than in Fig. 6, as expected. The second update sol-

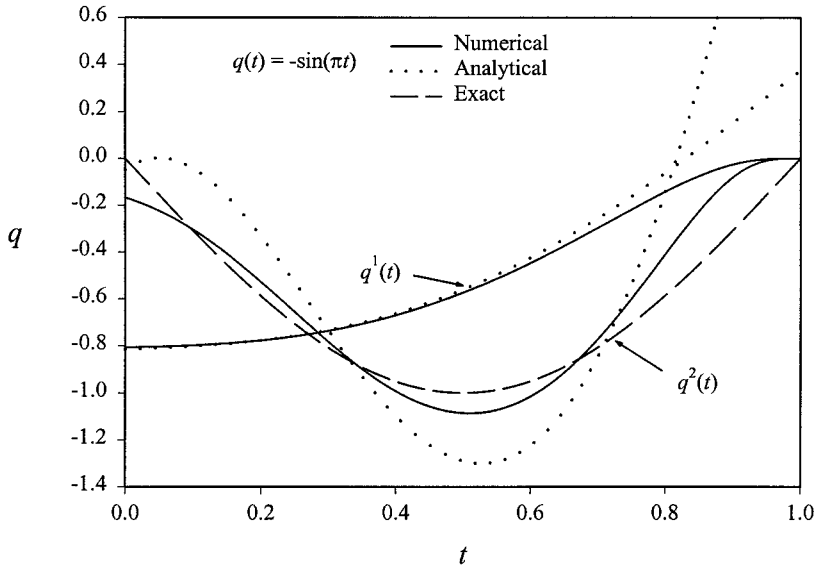

Fig. 5. Predicted fluxes for $\omega = \pi$ and $t_f = 1$.

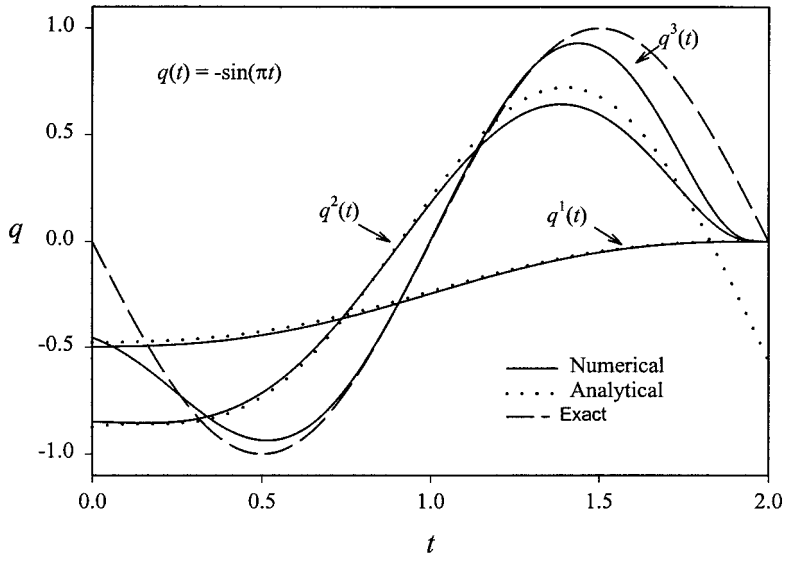

Fig. 6. Predicted fluxes for $\omega = \pi$ and $t_f = 2$.

ution behaves on the other hand not as a linear, but as a cubic polynomial in t, with coefficients inversely proportional to ω, in good agreement with Eq. (23). The solution at this early stage is still far from the exact sinusoidal solution. Convergence is nevertheless taking place in the process. It only occurs at a much slower rate. This is not surprising, since the adjoint temperature is inversely proportional to ω at any given iteration. In fact, the solution profile obtained after 20 iterations, for a sensor located at $x = 0$, has only roughly one third of the amplitude of the actual flux. It is feasible to speed up convergence by taking the sensor closer to the active boundary. Fig. 8 shows indeed that a fairly accurate solution (over most of the time interval) can be obtained after 20 iterations, using a centered sensor.

On the basis of the above discussion, let us now investigate what happens when the boundary flux

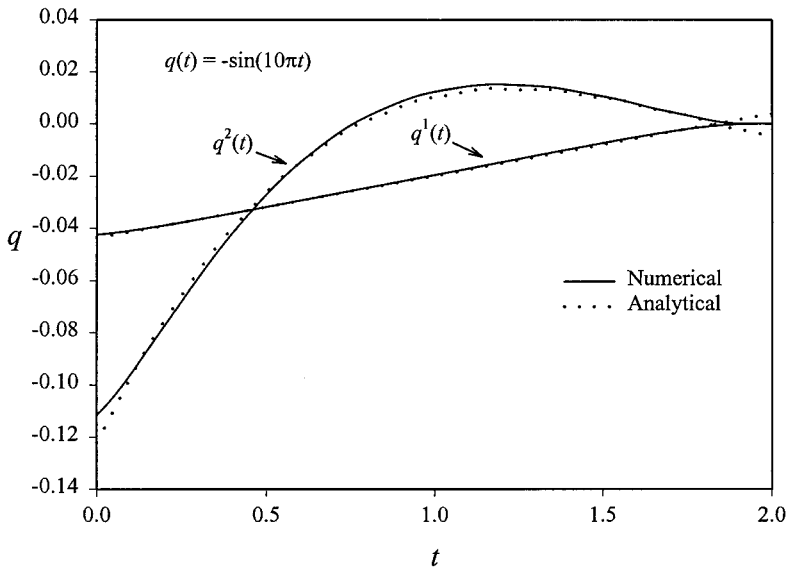

Fig. 7. Predicted fluxes for $\omega = 10\pi$ and $t_f = 2$.

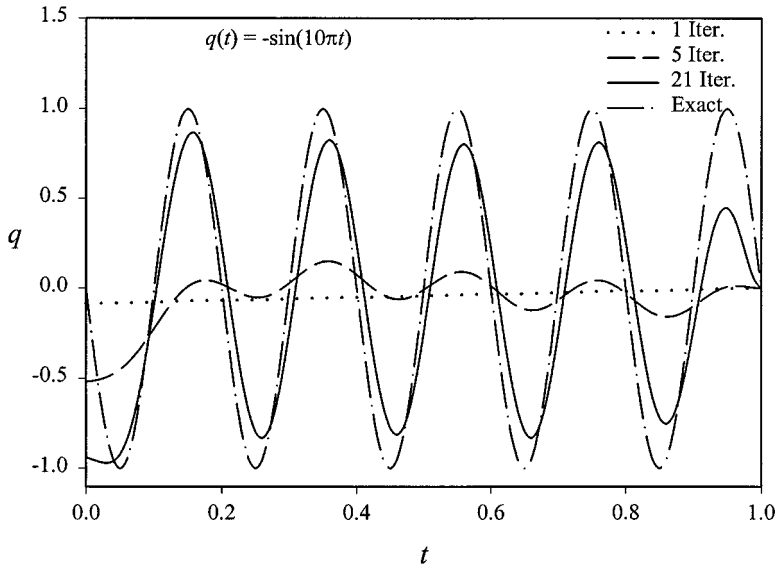

Fig. 8. Solutions for $\omega = 10\pi$ and centered sensor.

involves two different frequency components, by considering for instance

$$q(t) = -\sin(\omega t) - \sin(\omega/\varepsilon t) \tag{24}$$

where ε is a small number, say $\varepsilon < 0.1$. An adjoint temperature solution $\bar{T}^0$ is associated with each component, in which the terms involving D in Eq. (13) may be neglected for the ω/ε frequency component.

The first update q^1 is obtained by superposition of the solutions. The result involves both a linear term in t and an harmonic term in ωt, and therefore has the exact same form as the imaginary part of Eq. (16). The corresponding B_1 and C_1 coefficients are then given by

$$B_1 = ia_{11}\frac{\alpha^0}{\omega}(1+\varepsilon)$$

$$C_1 = -i\frac{\alpha^0}{\omega}\left((1+\varepsilon)P_1(t_f) + \frac{e^{i\omega t_f}}{D}\right) \tag{25}$$

The values of A_1 and α^0 remain essentially what they would be if the flux involved only the lower frequency component sin(ωt). It is clear from Eq. (25) that the influence of the higher frequency component on q^1 is of order ε. The same conclusions hold for the second update as well. It appears therefore that the algorithm generates for the first few iterations a series of updates $q^1, q^2, \ldots$, mainly associated with the lower frequency component of the flux. The various components are thus recovered from the lowest to the highest frequencies in a sequential manner.

This is confirmed in Fig. 9, where the solution profile q^2 for a flux $q(t) = -\sin(\pi t) - \sin(10\pi t)$ with a centered sensor is nearly identical with the corresponding plot in Fig. 5. The graph reproduces essentially the low frequency component $\omega = \pi$ of the flux. After 30 iterations, the high frequency component is well recovered, and the solution is then accurate.

The regularization property of the algorithm can be fully appreciated, as a certain level of white noise is purposely introduced in T_m, in order to simulate the errors encountered in actual field measurements. In this case E in Eq. (3) does not converge to zero, but to a value related to the statistical variance of the noise. Results obtained from the noisy data $T_m(1 + 0.03\sigma)$, where $|\sigma| < 1$ is a uniformly distributed random number, are presented next, for a flux $q(t) = -\sin(\pi t)$. For a centered sensor, the flux profile obtained after 20 iterations depicted in Fig. 10 clearly shows the presence of higher frequency components in the solution, which is no longer uniform along y. Slight variations in the data become critical in this context, and the coefficients α and γ must be computed with as much precision as possible. Considering the sequential convergence process described earlier, it is expected that there may be an optimal number of iterations leading to a reasonably accurate prediction of the unknown flux, before the higher frequency components of the noise are recovered and start to adversely affect the solution. Experimentation with the number of iterations reveals that a better solution is obtained after

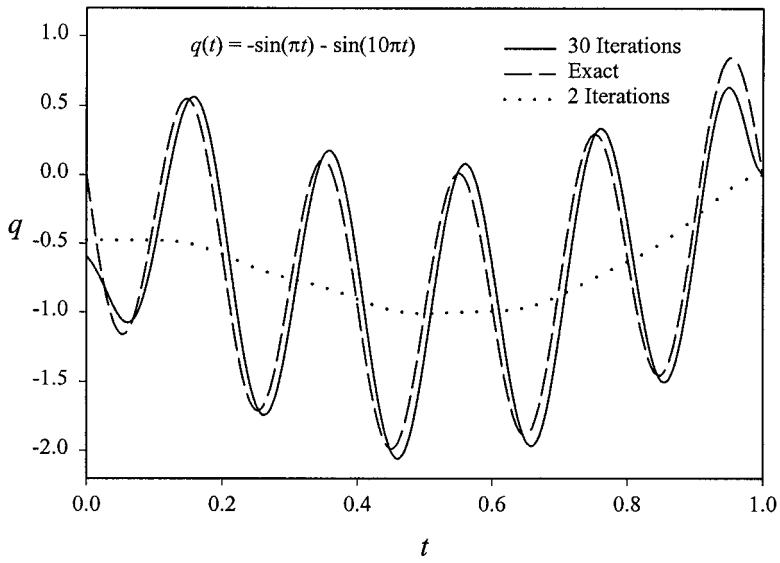

Fig. 9. Solutions for two frequency components and centered sensor.

three or four iterations indeed. This is confirmed in Fig. 11, where the graph appears smoother and closer to the exact solution profile. The determination of the optimal number of iterations is somewhat subjective. It will involve some a priori knowledge and trial and error. But experience suggests as a guideline to look at the first few solutions obtained immediately after the error residuals begin to level out.

The extent to which random noise will affect the solution is also strongly a matter of the sensor position.

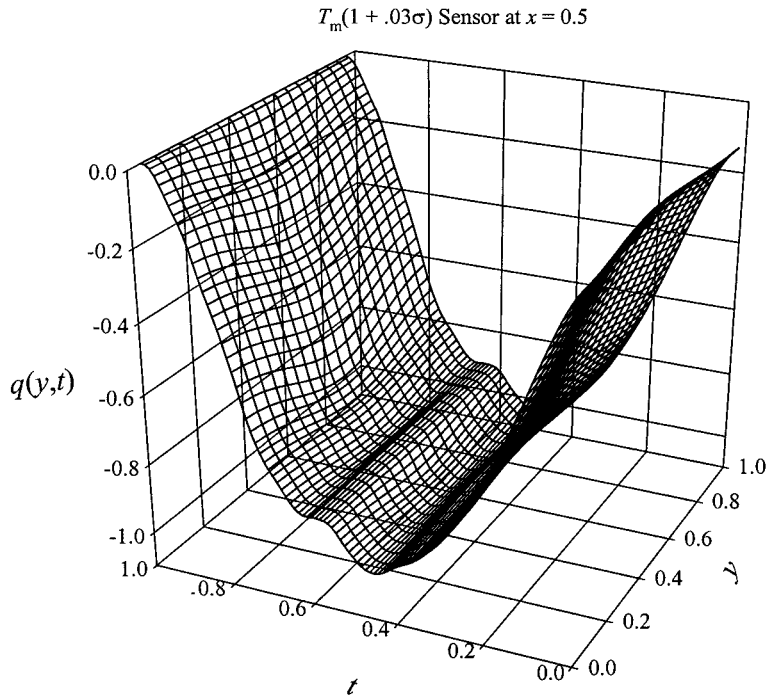

Fig. 10. Heat flux after 20 iterations. Noisy data and centered sensor.

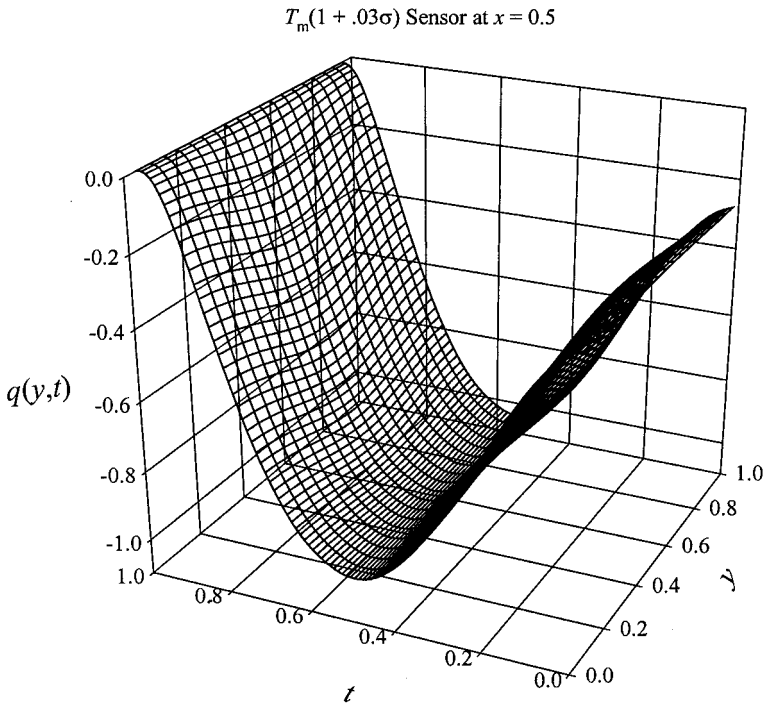

Fig. 11. Heat flux after three iterations. Noisy data and centered sensor.

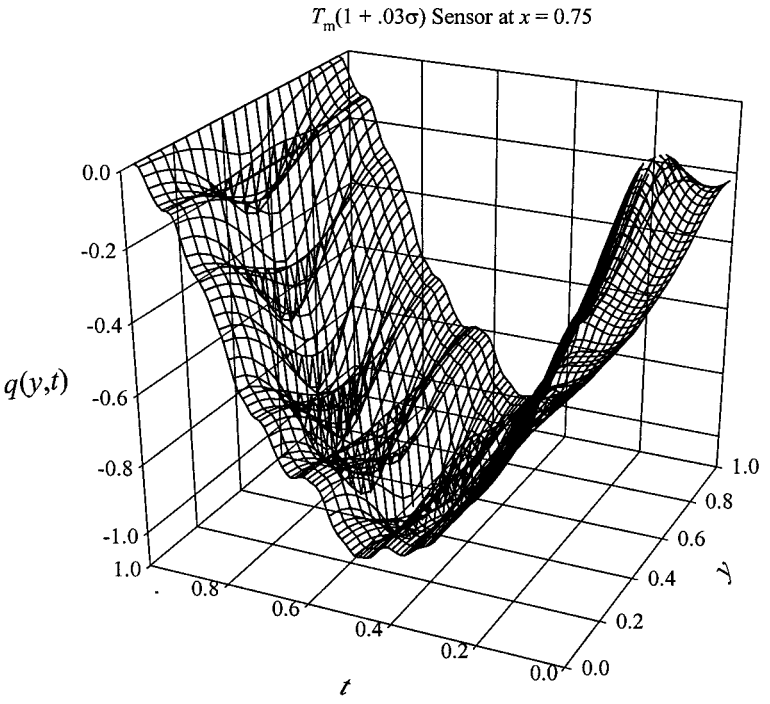

Fig. 12. Heat flux after 20 iterations. Noisy data with sensor at $x = 0.75$.

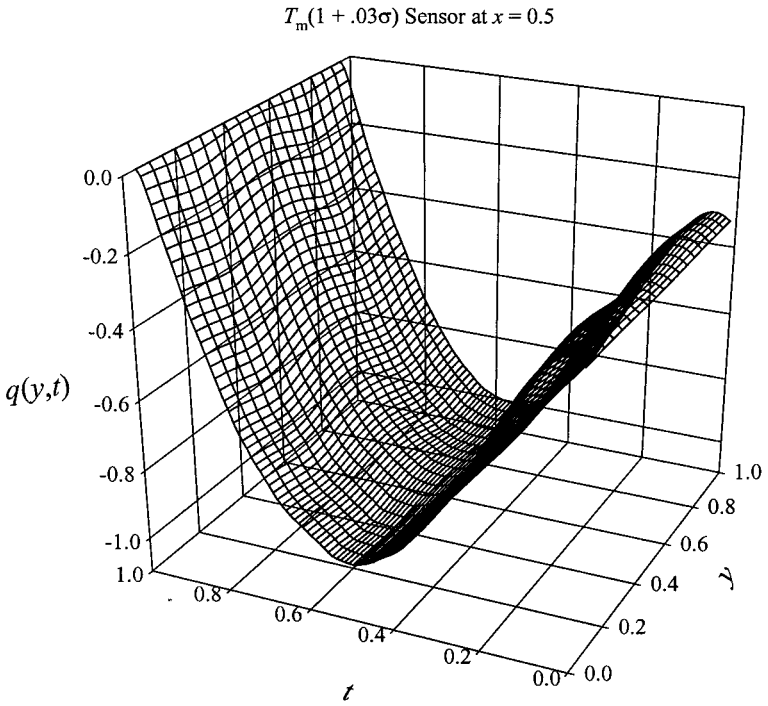

Fig. 13. Heat flux after three iterations. Noisy data with two sensors at $x = 0.75$.

If the sensor is placed near the active boundary, at $x = 0.75$ for instance, the sensitivity of the algorithm to the higher frequency components of T_m is greater. The consequences are obvious in Fig. 12, where the solution profile appears much more distorted than in Fig. 10 for a centered sensor, all other quantities being the same. In fact, a satisfactory solution can not be achieved after any number of iterations with a single sensor located at $x = 0.75$. Using 2 sensors at the same location, placed symmetrically at $y = 0.25$ and $y = 0.75$, will produce after 20 iterations a profile just as warped as for a single sensor. But the result after three iterations is strikingly different this time, as revealed in Fig. 13.

4.2. Two-dimensional case

When a non-uniform boundary condition such as

$$q(y) = 0, \quad 0.5<y<1$$

$$q(y) = \cos(\pi y), \quad 0<y<0.5 \tag{26}$$

is imposed at the left wall, the temperature field within the cavity will be two-dimensional and asymmetric. The unknown flux at the right wall may still be recovered using a single sensor, as long as it remains a function of time only. For a centered sensor, the converged solution is virtually undistinguishable from what is found when $q(y)=0$ at the left wall. This is so, because the symmetry of the adjoint solution is solely determined by the sensor's position within the cavity. It is not affected by the changes in the boundary conditions like Eq. (26).

It has been verified so far that sensitivity increases as the sensor is placed closer and closer to the active boundary. However, the positioning along y is also a significant parameter, as we shall see.

Fig. 14 provides a comparison of the flux profiles obtained at $t = 0.2$, 0.5, after 20 iterations, with sensors located at different vertical positions along the line $x = 0.5$, under otherwise identical conditions. The plots associated with the centered sensor appear nearly uniform at $t = 0.5$, but not at $t = 0.2$, where they show slight but perceptible variations. The solution obtained with two sensors placed symmetrically at $y = 0.25$ and $y = 0.75$ is for all practical purposes uniform along the y-coordinate, as it should, unlike the single-sensor solution. For a sensor placed at $y = 0.75$, the predicted profile is biased. The solution has the right shape at any given y position, but the amplitude is greater in the upper part of the cavity, where the sensor is located. The results obtained with a sensor located at $y = 0.25$ are symmetrical. Averaging them

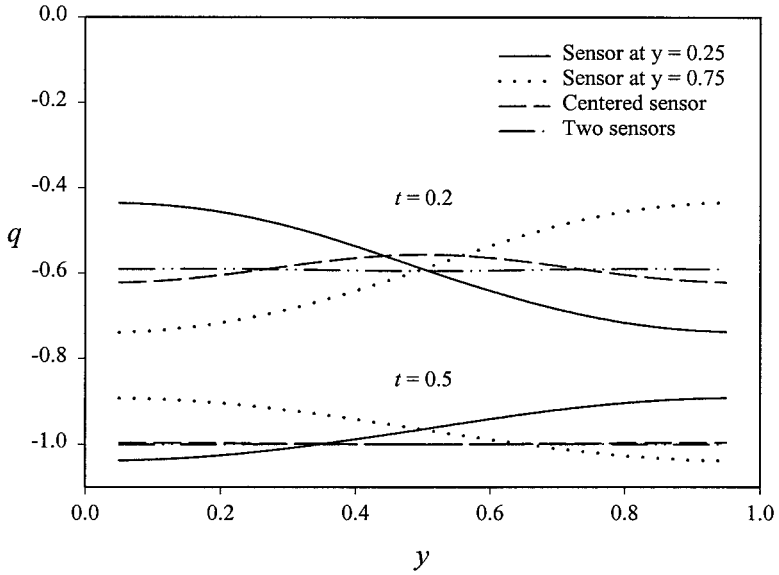

Fig. 14. Flux profiles for various sensor configurations at $x = 0.5$, 2D case.

would produce a solution close to the exact results $-\sin(\pi/5)$, -1 at $t = 0.2$ and 0.5, respectively.

5. Concluding remarks

A Fourier analysis of the IHCP solution was carried out in some details for the unknown heat flux $q(t)$, which shows that the convergence speed of the CGM algorithm slows down as frequency increases.

The algorithm has the ability to predict the various frequency components of a completely unknown heat flux in sequence, the lower frequencies being recovered first. This sequential convergence process is at the origin of the regularisation mechanism of the method. Satisfactory predictions of a time-dependent heat flux were obtained from either exact or noisy data after an optimal number of iterations.

A single sensor may be used in both one- and two-dimensional cases, but using a pair gives additional stability and better uniformity. In any case, the sensor(s) should be placed in a symmetric way within the cavity to achieve good results.

Acknowledgement

This research was supported by the Natural Sciences and Engineering Research Council of Canada.

Appendix A

Direct problem

Let $F(x,s)$ and $Q(s)$ be the Laplace transforms of $T(x,t)$ and $q(t)$, respectively. In the transformed domain, the direct problem Eq. (2) reduces to

$$F'' - sF = 0; \quad F'(0) = 0, F'(1) = -Q(s) \tag{A1}$$

which has the solution

$$F(x, s) = -\frac{Q(s)\cosh(s^{1/2}x)}{s^{1/2}\sinh(s^{1/2})} \tag{A2}$$

The expression can be transformed back to the time domain, using the standard inversion technique with residues. This gives

$$T(x, t) = \sum_{\text{Res}} F(x, s)\mathrm{e}^{st} \tag{A3}$$

Let $q(t) = t^n$, for instance, with the transformation $Q = n!/s^{n+1}$. The computation of $T(0,t)$ from Eq. (A3) will thus require the evaluation of the residues of

$$F(s)\mathrm{e}^{st} = -\frac{n!\mathrm{e}^{st}}{s^{n+3/2}\sinh(s^{1/2})} \tag{A4}$$

The poles at $s = -n^2\pi^2$, $n = 1, 2, 3\ldots$, are of order one. They are associated with temperature transients. The pole at $s = 0$, on the other hand, is of order $n + 2$, as can be seen using the expansion

$s^{1/2}\sinh(s^{1/2}) = s(1 + s/3! + s^2/5! + \ldots)$ in Eq. (A4). The residue is computed as

$$\text{Res} = \lim_{s\to 0}\frac{1}{(n+1)!}\,\frac{\mathrm{d}^{n+1}}{\mathrm{d}s^{n+1}}\{s^{n+2}F(s)\mathrm{e}^{st}\} = \lim_{s\to 0}\frac{1}{n+1}\,\frac{\mathrm{d}^{n+1}}{\mathrm{d}s^{n+1}}\left\{\frac{-\mathrm{e}^{st}}{(1 + s/3! + \ldots)}\right\} \tag{A5}$$

where $P_1(t)$, $P_2(t)$, $P_3(t)$, …, etc. are polynomials of degree 1, 2, 3, …, and so on. Let us define for $n = 1, 2, \ldots$ the polynomial of degree n as

$$P_n(t) = \sum_{m=0}^{m=n} a_{nm}t^m \tag{A6}$$

The coefficients a_{ij} up to the fourth order are

$$\begin{aligned} &a_{11} = -1 \quad a_{10} = \tfrac{1}{6} \quad a_{22} = \tfrac{-1}{2} \quad a_{21} = \tfrac{1}{6} \\ &a_{20} = \tfrac{-7}{360} \quad a_{33} = \tfrac{-1}{3} \quad a_{32} = \tfrac{1}{6} \quad a_{31} = \tfrac{-7}{180} \\ &a_{30} = \tfrac{31}{7560} \quad a_{44} = \tfrac{-1}{4} \quad a_{43} = \tfrac{1}{6} \quad a_{42} = \tfrac{-7}{120} \\ &a_{41} = \tfrac{31}{2520} \quad a_{40} = \tfrac{-127}{100{,}800} \end{aligned} \tag{A7}$$

Adjoint and sensitivity problems

With $F(x, s)$ and $Q(s)$ as the transforms of $\bar{T}(x, \tau)$ and $T - T_{\mathrm{m}}(\tau)$, respectively, the adjoint problem becomes

$$F'' - sF = 0; \quad F'(0) = Q(s), F'(1) = 0 \tag{A8}$$

in the s domain, for a sensor placed on the left boundary, with the solution

$$F(x, s) = -\frac{Q(s)\cosh[s^{1/2}(1 - x)]}{s^{1/2}\sinh(s^{1/2})} \tag{A9}$$

Specializing the latter at $x = 1$, it becomes clear that both $\bar{T}(1, \tau)$ and $T(0, t)$ are obtained by inverting formally identical expressions. If the same $Q(s)$ is given for both, the results are the same also. The adjoint temperature profile at the active boundary can thus be deduced from previous direct problem solutions, using symmetry and superposition.

The sensitivity problem is governed by the same equation and boundary conditions as the direct problem. Let $Q(s)$ stand for the transform of $p(t)$ this time. It follows from the same argument that $\bar{T}(0, t)$ is given by the inverse of Eq. (A2) evaluated at $x = 0$.

References

[1] J.V. Beck, B. Blackwell, C.R. St-Clair Jr, Inverse Heat Conduction: Ill-Posed Problems, Wiley Interscience, New York, 1985.

[2] O.M. Alifanov, Inverse Heat Transfer Problems, Springer-Verlag, Berlin Heidelberg, 1994.

[3] J. Hadamard, Lecture on Cauchy's Problem in Linear Partial Differential Equations, Yale University Press, 1923.

[4] N.H. Dinh, Methods for Inverse Conduction Problems, Peter Lang, Frankfurt, Bern, New York, Paris, 1998.

[5] Y. Jarny, M.N. Ozisik, J.P. Bardon, A general optimization method using adjoint equation for solving multidimensional inverse heat conduction, Int. J. Heat Mass Transfer 34 (11) (1991) 2911–2919.

[6] R.A. Meric, Optimization of thermal conductivities of isotropic and orthotropic solids, J. Heat Transfer 107 (1985) 508–513.

[7] T.H. Nguyen, An optimization approach to some inverse convection problems, in: Proceedings of International Conference on Analysis and Mechanics of Continuous Media, Ho-Chi Minh City, 1995, pp. 188–195.

[8] M. Prud'homme, T.H. Nguyen, Whole time-domain approach to the inverse natural convection problem, Num. Heat Transfer 32 (1997) 169–186 (Part A).

[9] R. Fletcher, Practical Methods of Optimization, John Wiley & Sons, New York, 1987.

[10] M. Prud'homme, Optimisation du problème de conduction inverse par le gradient conjugué. Report EPM/RT-98/11 (1998).

[11] J. Chen, Inverse heat conduction problem in a cavity. M.Sc.A. thesis Mechanical Engineering, Ecole Polytechnique de Montréal (1998).